**Light Metals 2012** *Edited by: Carlos E. Suarez*
***TMS (The Minerals, Metals & Materials Society), 2012***

# ELECTROMAGNETIC AND MHD STUDY TO IMPROVE CELL PERFORMANCE OF AN END-TO-END 86 KA POTLINE

Amit Gupta[1], Manoj Chulliparambil[1], Sankar Namboothiri[1], Satheesh Mani[1], Biswajit Basu[1] and Jinil Janardhanan[2],
[1]Aditya Birla Science and Technology Company Ltd, Plot No 1 & 1- A/1, MIDC, Taloja, Panvel, Raigad, Maharashtra, 410208, India
[2]Hindalco Industries Ltd, Hirakud, Sambalpur, Orissa, 768016, India

Keywords: Electromagnetic model, Magnetic compensation, MHD model

## Abstract

Electromagnetic forces in the electrolyte and metal pad region of aluminum reduction cells affect the metal/electrolyte flow pattern and hence the cell performance, indicated by current efficiency and specific energy consumption. Numerical simulation has become an effective tool for analyzing such complex physics. In this paper, an electromagnetic and MHD study conducted for an 86 kA end-to-end potline is described. A detailed three-dimensional electromagnetic model was built in commercial ANSYS software package and steady state MHD (velocities and metal heave) in the cell were computed using CFX software. Magnetic field from the model was validated with the plant measurements. Various busbar configurations were analyzed using the developed model. The results show that new magnetic compensation designs effectively improve the magnetic field, the metal flow profile and the metal heave, thereby providing conditions for improving cell performance.

## Introduction

Primary aluminium metal is industrially produced in aluminium smelters by Hall-Héroult process. In a smelter there are several electrochemical cells or pots, connected in series to form one or more potlines. The pots in a potline are connected by aluminium busbars and DC current flows from one pot to another in these busbars. Within a pot, the current flow downwards through carbon anodes, molten cryolite bath, molten aluminium metal and then to carbon cathode blocks. Steel collector bars embedded in the cathode take the current out from the cathode blocks to the busbars which lead to the next pot. Strong magnetic fields are also generated in and around the pot due to the flow of electric current through the potline components. Cryolite bath and the metal are two immiscible liquids and the bath floats on top of the metal due to its slightly lower density compared to the metal. Undisturbed metal-bath interface would be flat and horizontal, but this is not the case in an operating aluminium reduction cell. Combination of the electric current and the magnetic field gives volumetric forces, known as Lorentz or electromagnetic forces. These forces are responsible for movement of the metal and the bath as well as for deformation of the metal-bath interface. Magnetohydrodynamics (MHD) is the science that studies the effect of electromagnetic forces on fluid flow.

Cryolite bath is a poor conductor of electricity and the bath layer is the region of maximum ohmic heat generation within the cell. The ohmic heat generated in the bath layer is proportional to the anode-to-cathode distance (ACD) and therefore it is desirable to maintain this layer as thin as possible subject to satisfying the heat balance constraint. However, maintaining a thinner ACD is often constrained by instability induced by waves generated from the unbalanced magnetic field. The instability at a lower ACD may cause metal shorting with the anode, leading to loss in current efficiency. The minimum ACD at which the cell remains stable depends on factors such as cell design, busbar design and cell operation. Cell amperage also plays a major role since electromagnetic forces in the liquid region of the pot increases approximately as square of the current. The limiting factors of amperage increase considerations in a potline are largely determined by the MHD stability to maintain a lower ACD and heat balance of the cell [1]. Hence, thorough understanding of the cell MHD for appropriate design and control is a key to achieve high energy efficiency.

In this study, a 3-dimensional electromagnetic and a steady state MHD model for an end-to-end 86 kA potline was developed using ANSYS and CFX commercial software packages. The electromagnetic and the magnetohydrodynamic parts were solved with ANSYS and CFX respectively. For simplification, influence of bubbles generated by the anode reaction on the bath flow was not taken into account in this analysis. Several simulations were run to obtain an optimum magnetic compensation, which resulted in a balanced metal flow profile and a flatter bath-metal interface.

## Model Description

As discussed in the last section, magnetic field plays a major role in the performance of an aluminum electrolysis cell. Even small variations of busbar configuration have strong influence on the multiple physical fields and these are studied using computer simulations of base electromagnetic model of the cell. In this study, meshing for the electromagnetic model was made in ANSYS and meshing for the MHD model was made in ICEM-CFD. Different mesh was used for each step as ANSYS use finite element method and CFX use finite volume method for calculations. Electrical and magnetic calculations were done assuming that interface between the metal and the bath is flat. Steady state MHD simulations with flat anodes were run in CFX with the volumetric electromagnetic force obtained from ANSYS [2]. The electromagnetic and the MHD model development are described separately in the next two subsections.

### Electromagnetic Model

First step in the MHD modeling is to develop a detailed full cell 3-D electromagnetic model. All relevant aspects of the cell, such as external conductors (busbar arrangement), internal conductors (liquid layers, collector bars, anodes and cathodes), and steel potshell were taken into account. For electromagnetic analysis, firstly electric current distribution was solved by application of the Ohm's Law.

$$\mathbf{J} = -\sigma \nabla V \qquad (1)$$

Since electric current is conserved within the cell:

$$\nabla . \mathbf{J} = 0 \tag{2}$$

Accordingly,

$$\nabla . (\sigma \nabla V) = 0 \tag{3}$$

Which is the Laplace equation in electric potential '$V$' and this can be solved with appropriate boundary conditions. In Equations (1) – (3), $\sigma$ is the electrical conductivity (S/m) and **J** is the current density vector (A/m$^2$). The boundary conditions used were: (a) reference potential equal to zero at negative terminal of the power supply and (b) pot line current entering at the positive terminal.

In computation of the electromagnetic fields, coupled interaction among multiple physical field in the cell such as thermal and fluid flow effects were not considered. The general magnetic scalar potential approach works well for electrolysis cells in order to account for electrical current going out through the cathode and this approach was used here [2]. The model was solved in ANSYS and brief descriptions of equations which were solved are as follows. The "initial guess" field $\mathbf{H_g}$, is calculated from the Biot-Savart integration, by Equation (4).

$$\mathbf{H_g} = \frac{1}{4\pi} \iiint_{volC} \frac{\mathbf{J} \times \mathbf{r}}{\mathbf{r}^3} d(volC) \tag{4}$$

$\mathbf{H_g}$ is the preliminary magnetic field from electric current sources (conductors), **J** is the current density in the conductor, *volC* is the volume of the conductor and **r** is the distance vector between the conductor and the point of interest. The constitutive relationship for magnetic fields is given by Equation (5).

$$\mathbf{B} = \mu \mathbf{H} \tag{5}$$

Where, **B** is the magnetic induction (T), **H** is the magnetic field strength (A/m) and $\mu$ is the magnetic permeability. **H** is calculated from Equation (6).

$$\mathbf{H} = \mathbf{H_g} - \nabla \emptyset_g \tag{6}$$

Where, $\emptyset_g$ is the generalized magnetic scalar potential, which is calculated from Equation (7).

$$\nabla . \mu \nabla \emptyset_g - \nabla . \mu \mathbf{H_g} = 0 \tag{7}$$

In ANSYS, the solid element, SOLID98, which is capable of electrical and magnetic calculation, was used for defining the cells (analyzed and neighbouring cell) and the busbar network was modeled using the line element, LINK68, which is capable of electrical calculations only. The above methodologies (SOLID98 and LINK68) are described in detail elsewhere [3]. Surrounding the cell of interest, an amount of air was modeled by considering sufficient elements to accurately define the magnetic scalar potential gradient. The boundary condition "Normal Flux" (which implies magnetic field lines are normal to the applied face) was applied in external nodes of the air box. A Full cell 3-D electromagnetic model was developed using APDL (ANSYS Parametric Design Language) which is advantageous for quicker parametric analysis in pre-and-post processing of the simulation.

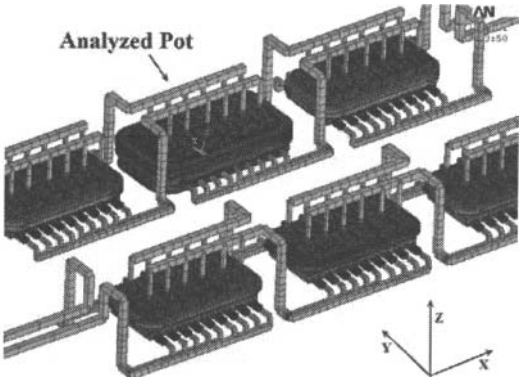


Figure 1: Electromagnetic model geometry and mesh

Figure 1 shows part of the mesh used in the electromagnetic model. As shown, magnetic field from the neighbouring cells were also considered in the model. Magnetic field from the neighbouring potline was accounted by assuming the neighbouring potline as a straight conductor carrying the line current. In neighbouring row of the pots, three nearest pots were modeled in detail. The coordinate system was taken such that origin is at bottom-center of potshell of the analyzed pot, x-axis is along long side of the pot (defining upstream end of the pot in negative x-direction and the downstream end in positive x-direction), y-axis is along short side of the pot and z-axis is vertically upwards (as shown in Figure 1).

In order to understand the effect of steel potshell, first electromagnetic model was developed for calculation of the magnetic field considering only the current carrying conductors. Once these results were found and analyzed, the steel shell (ferromagnetic material effect) was incorporated into the model and the magnetic field was once again computed. This was taken as the base case for further magnetic study including magnetic compensation. Magnetic field, electric current density and electromagnetic force obtained from the electromagnetic model were transferred seamlessly from ANSYS to CFX.

Steady Sate MHD Model

Steady state MHD models play an important role in the cell MHD design, since it gives relevant information about the mean values of the liquid flow and extent of deformation of the metal-bath interface [2]. It is also useful to determine alumina point feeder positions to maximize alumina mixing within the bath. It is well known that in solution of MHD flow problems, the Navier-Stokes equation and the Maxwell equations are coupled through the expression for the Lorentz force [2]. Volumetric electromagnetic forces in the liquids are obtained as vector product of the current density and the magnetic field as follows.

$$\mathbf{F}_{EM} = \mathbf{J} \times \mathbf{B} \tag{8}$$

In CFX, the main sets of equations solved are the Navier-Stokes equation and the continuity equation.

$$\rho \left( \frac{\partial \mathbf{v}}{\partial t} + \mathbf{v} . \nabla \mathbf{v} \right) = -\nabla p + \nabla \left( \mu_{eff} \nabla \mathbf{v} \right) + \rho \mathbf{g} + \mathbf{F}_{EM} \tag{9}$$

$$\nabla . \mathbf{v} = 0 \tag{10}$$

Where, **v** is the velocity (m/s), $p$ is the pressure (Pa or N/m$^2$), $\mu_{eff}$ is the effective dynamic viscosity (Pa.s), $\rho$ is the density (kg/m$^3$), $\mathbf{F}_{EM}$ is the electromagnetic force (N/m$^3$) and **g** is the gravity (9.8 m/s$^2$).

Some of the major considerations/assumptions used for developing the MHD model are given below:

- Fluid domain considered for MHD model was molten bath and the metal.
- The fluid boundaries; upper side of channels formed in-between the anodes and formed between the cell sidewall and the anodes were treated as open boundaries. All other boundaries were set to have no slip boundary condition [4].
- Constant turbulent viscosity model was used which provide more close prediction to the real cell [4].
- The bath-metal flow was solved using the Euler-Euler homogeneous model, where, a common flow field as well as other relevant fields such as pressure and turbulence is shared by all the fluids [3].
- For the interface tracking, Volume of Fluid (VOF) method was used. Shape of the interface was given by the geometric location of the finite volumes with 0.5 of volume fraction of each liquid.

In this paper, MHD results are shown for the base case (i.e. present busbar) and also a comparison was made between the base case and a modified busbar configuration for the pot.

## Results and Discussion

Electromagnetic Model Results

The magnetic field values at the middle height of the metal pad and along length of the pot in x-direction are extracted from the model results. In the result plots shown here, magnetic field values are plotted at y = ± 1.2 m, which corresponds to the anode edge near the sidewall of the pot and at y = 0, which corresponds to the centerline of the pot.

Figures 2, 3 and 4 show the magnetic field components in absence of the steel shell. Figure 2 shows that the longitudinal magnetic field component $B_x$ is symmetrical about x-axis of the pot which is desirable as it will keep transverse metal heaving to a minimum and symmetrical across the length of the pot.

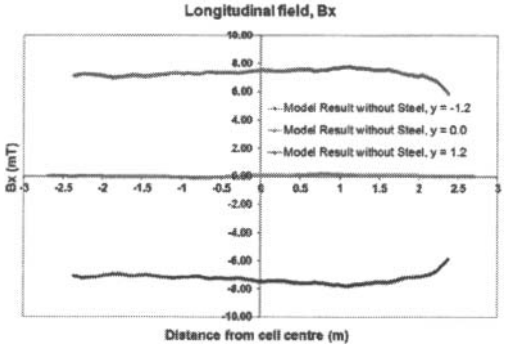


Figure 2: Longitudinal magnetic field without steel shell (mT)

Figure 3 illustrates that transverse magnetic field component $B_y$ has higher magnitude on upstream side (current entry side) of the pot compared with downstream side (current exit side).

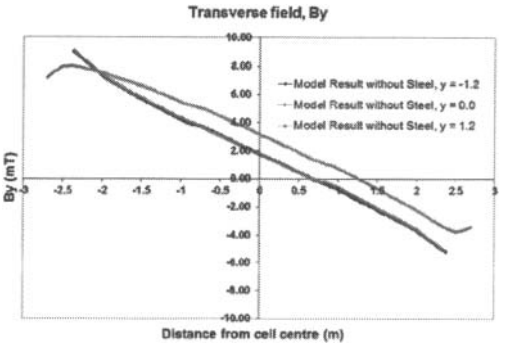


Figure 3: Transverse magnetic field without steel shell (mT)

Figure 4 shows that vertical magnetic field component $B_z$ is unsymmetrical along x and y axis. It indicates that the component $B_z$ in the metal pad is affected by the neighbouring pot rows which induces a negative bias. Cathode busbars (carrying horizontal current) are prime producer of vertical magnetic field at the metal pad level.

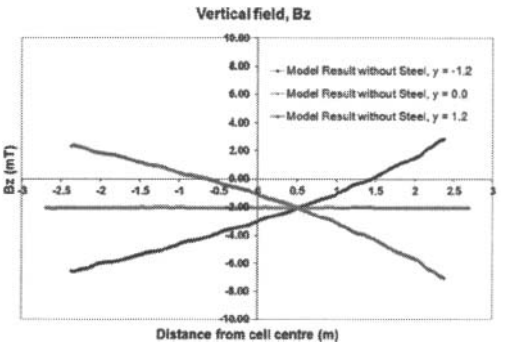


Figure 4: Vertical magnetic field without steel shell (mT)

The Figures 5, 6 and 7 shows the three components of magnetic field in presence of the steel shell. The results demonstrate that the steel shell provides a shielding effect by reducing overall magnitude of the transverse magnetic field component $B_y$ and making the vertical magnetic field component $B_z$ more symmetrical.

Figure 5 illustrates that in presence of the steel shell, longitudinal magnetic field component $B_x$ remains symmetrical about x-axis of the pot.

Figure 6 shows that transverse magnetic field component $B_y$ has a higher magnitude on the upstream side compared with the downstream side with overall reduction in magnitude due to presence of the steel shell. The higher magnitude of transverse magnetic field on the upstream side is responsible for longitudinal metal heaving towards the downstream end of the pot.

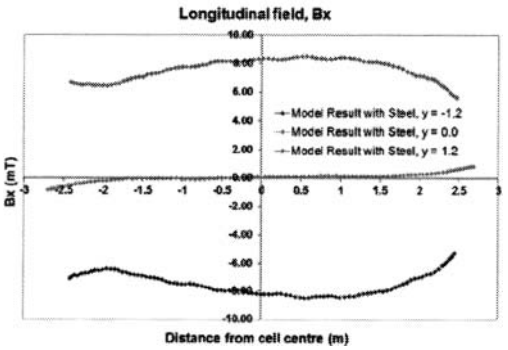


Figure 5: Longitudinal magnetic field with steel shell (mT)

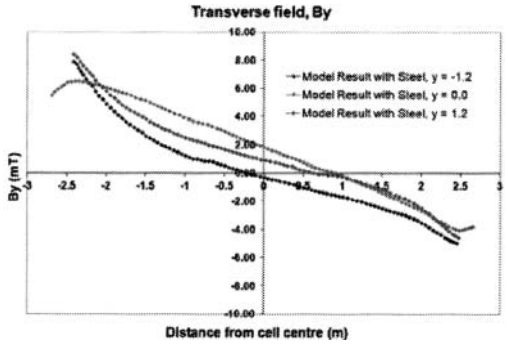


Figure 6: Transverse magnetic field with steel shell (mT)

Figure 7 illustrates that the vertical magnetic field component $B_z$ is unsymmetrical along x and y axis. In presence of the steel shell, the component $B_z$ at y = + 1.2 m is found to have a more positive value compared with the simulation without the steel shell. However, the values at y = - 1.2 m are less affected by presence of the steel shell. This shows that the steel shell helps in making the field more symmetrical, thus providing some shielding effect.

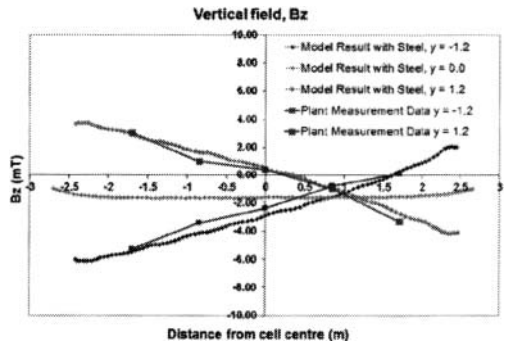


Figure 7: Vertical magnetic field with steel shell (mT)

Electromagnetic Model Validation

In order to validate the magnetic field results obtained from the model, a measurement campaign was conducted in a representative pot of an 86 kA potline. The measurements were conducted in side channel of the pot and near the anode edge (y = ± 1.2 m) at middle height of the metal pad. A jack hammer was used to create holes in the anode cover/crust for conducting the measurements. An in-house developed air cooled thermal shielding device was used to protect the uniaxial $B_z$ probe during the magnetic field measurement in the running pot. The measurements were also repeated to confirm the repeatability of the values obtained. Figure 8 shows that the vertical magnetic field component $B_z$ measured inside the pot and results of the electromagnetic model with the steel shell are in close conformance.

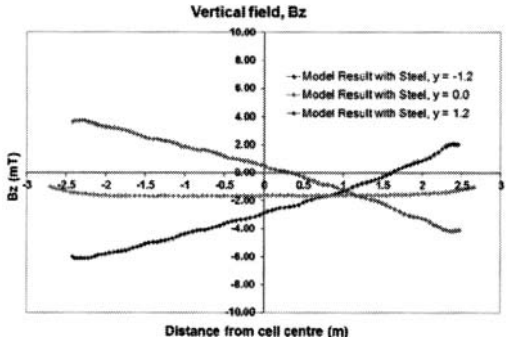


Figure 8: Comparison between plant measurement data and the model results for vertical magnetic field (mT)

Magnetic Compensation

The base model was used for simulating different magnetic compensation schemes. The analysis focused basically on two schemes: 1) Introducing compensatory current loop and 2) compensation using rearrangement of cathode busbar for dual-end current entry into the pot (asymmetric busbar configuration) [5]. The compensatory current loop investigated consist of an inner loop facing the neighbouring potline and outer loop facing the gallery as shown in Figure 9.

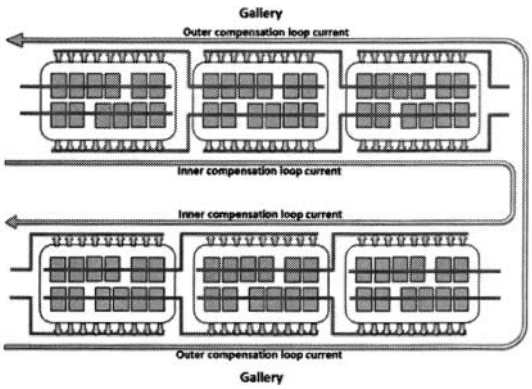


Figure 9: Schematic of potline with inner compensation loop and outer compensation loop

It was found that, the compensation loops do not have much effect on the longitudinal and the transverse magnetic field components. However, it shows significant effect on the vertical field. Figure 10 shows a comparison of the vertical magnetic field obtained among the existing busbar configuration, the inner compensation loop and the outer compensation loop. It also shows that more magnetic compensation of the vertical field can be achieved by

employing the outer compensation loop in comparison with the inner compensation loop.

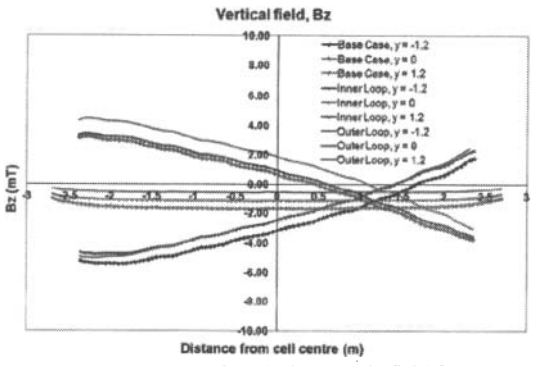


Figure 10: Comparison of vertical magnetic field for present busbar configuration, inner and outer compensation loop (mT)

The second scheme (asymmetric busbar configuration) used for simulation is shown in Figure 11. In this configuration, an additional busbar is introduced which is carrying some part of the current coming out of the cathode collector bars and this part is routed to the downstream end of anode beam of the next pot through an additional anode riser. This scheme provides dual end current entry into the pot.

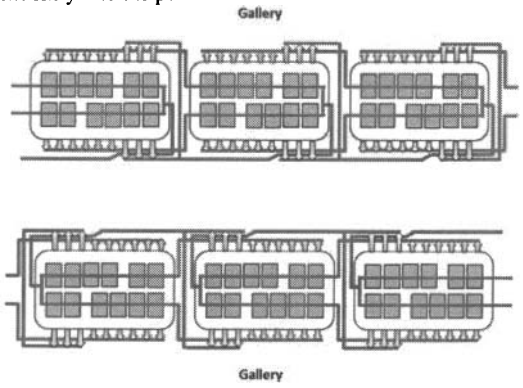


Figure 11: Schematic of asymmetric busbar configuration

Figure 12 show that the vertical magnetic field has become more symmetrical with the asymmetric busbar configuration.

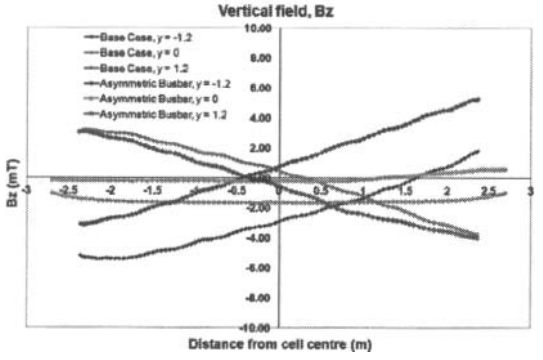


Figure 12: Vertical magnetic field comparison for present busbar and asymmetric busbar configuration (mT)

Figure 13 shows comparison of the transverse magnetic field between the existing busbar and the asymmetric busbar configurations. This scheme is shown to have double benefits as it provide compensation for the vertical magnetic field arising from the neighbouring pot row and also at the same time balancing the transverse magnetic field, which is responsible for longitudinal metal heaving.

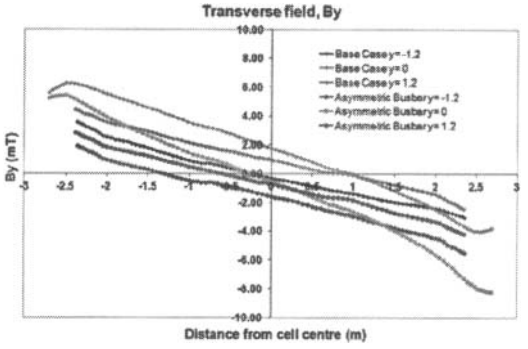


Figure 13: Transverse magnetic field comparison for present busbar and asymmetric busbar configuration (mT)

Steady State MHD Results

Figure 14 shows shape of the steady state metal-bath interface which indicates that the metal heaving is greater towards the downstream end with approximately 5.5 cm of interface deformation. Here, longitudinal hump near the downstream end is caused by the unsymmetrical transverse magnetic field (which was shown in Figure 6).

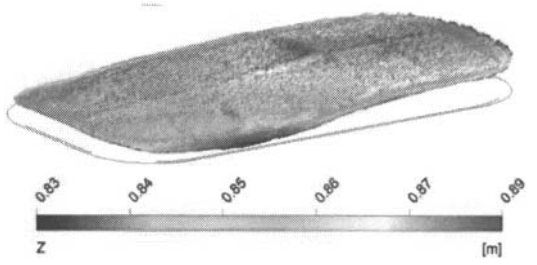


Figure 14: Steady state metal-bath interface shape (m)

Figures 15 and 16 show the steady state flow pattern of the metal and the bath respectively. From the figures, it is evident that the bath flow is essentially coupled to the metal flow and it is difficult to slow down the metal without slowing down the bath. Also, Figure 15 shows that a bigger diagonal pool has formed in the metal pad which is essentially because of the uncompensated magnetic field generated by the neighbouring potline [2]. Hence, MHD results of the base model further confirm uncompensated vertical magnetic field and unsymmetrical transverse field prevailing in the pot.

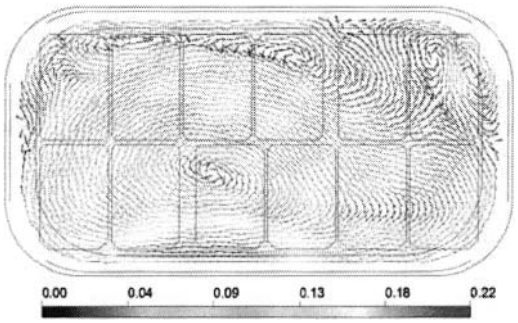


Figure 15: Steady state flow pattern at middle of metal pad (m/s)

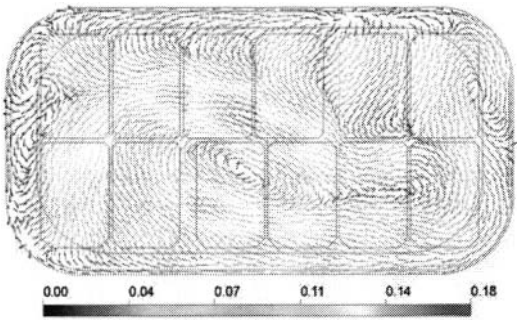


Figure 16: Steady state flow pattern at middle of ACD (m/s)

Table 1 shows the comparison of salient features of the MHD model results with the present busbar (base case) and with the asymmetric busbar configuration.

Table 1: MHD parameters comparison in metal pad

| Parameters | Present Busbar | Asymmetric Busbar |
|---|---|---|
| Average velocity | 5.9 cm/s | 5.0 cm/s |
| Maximum velocity | 21.9 cm/s | 12.8 cm/s |
| Percentage above 10 cm/s | 27.0 % | 9.6 % |
| Percentage below 5 cm/s | 37.9 % | 43.7 % |
| Metal heave (max–min) | 5.5 cm | 3.5 cm |
| Location of metal heaving | Near downstream end of pot | Near center of the pot |

From the Table, it can be seen that the metal velocity becomes more uniform and lower in magnitude with the asymmetric busbar configuration. Lower metal velocity reduces the back reaction and helps in improving the current efficiency. As discussed previously, the bath flow is coupled with the metal flow and hence the asymmetric busbar configuration also leads to a uniform flow profile in the bath. A uniform flow profile of the bath is desirable to achieve a consistent alumina concentration in the pot.

The next step in this study is to conduct the metal velocity and the interface profile measurements using iron rods in a few representative pots for validation of the MHD model. The metal velocity and the interface profile measurement using iron rod is described elsewhere [6,7]. This will be followed by implementation of the proposed busbar modification in the potline. These aspects will be discussed in a different paper.

## Conclusions

Three dimensional electromagnetic model (with and without steel potshell) and MHD model of an 86 kA pot in an end-to-end potline were developed. The electromagnetic base model results were validated with the magnetic field measurements conducted in a representative pot. The present busbar configuration provides an uncompensated vertical magnetic field and an unsymmetrical transverse field. The MHD model results for the present busbar configuration show metal heaving towards the downstream end, which further confirms the unsymmetrical transverse field. Simulation of the base model for magnetic compensation shows that an asymmetric busbar configuration provides the necessary compensation for vertical magnetic field from the neighbouring potline and makes the transverse magnetic field more symmetrical. The MHD results show that a more uniform flow profile with a lower metal velocity could be achieved by employing the asymmetric busbar configuration. Also with the asymmetric configuration the metal heaving is shifted to center of the pot with an overall lowering of the interface deformation as compared to the base case.

## Acknowledgement

The authors would like to thank Hindalco-Hirakud team for their help and support in conducting this study. The authors also wish to acknowledge Dr. Vinko Potocnik for his contribution to model verification and validation and also for many discussions during the course of this study.

## References

1. Vinko Potocnik, "Modeling of metal-bath interface waves in Hall-Heroult cells using ESTER/PHOENICS," Light Metals, TMS, (1989), 227-235

2. Dagoberto S. Severo, André-Felipe Schneider,, Elton C.V. Pinto, Vanderlei Gusberti, and Vinko Potocnik, "Modeling magnetohydrodynamics in aluminum reduction cell using Ansys and CFX," Light Metals, TMS, (2005), 475-480

3. ANSYS Inc Help Manual, Release 13.

4. Dagoberto S. Severo., Vanderlei Gusberti, Andre-Felipe Schneider,, Elton C.V. Pinto, and Vinko Potocnik,"Comparison of various methods for modeling the metal-bath interface," Light Metals, TMS, (2008), 413-418

5. Anthony R. Kjar, Jeffrey T. Keniry, and Dagoberto S. Severo, "Evolution of busbar design for aluminium reduction cells," 8th Australasian Aluminium Smelting Technology Conference, (2004)

6. Vinko Potocnik, and Frederic Laroche, "Comparison of Measured and Calculated Metal Pad Velocities for different prebake cell Designs," Light Metals, TMS, (2001), 419-425

7. Brian F. Bradley, Ernie W. Dewing and John N. Rogers, "Metal Pad Velocity Measurements by the Iron Rod Method,"Light Metals, 1984, 541-552.